Full Paper

CONTRAST MEDIA & MOLECULAR IMAGING

Received: 12 September 2013, Revised: 19 March 2014, Accepted: 25 March 2014, Published online in Wiley Online Library

(wileyonlinelibrary.com) DOI: 10.1002/cmmi.1606

Gallium(III) complexes of NOTA-bis (phosphonate) conjugates as PET radiotracers for bone imaging

Jan Holub[a], Marian Meckel[b], Vojtěch Kubíček[a], Frank Rösch[b] and Petr Hermann[a]*

Ligands with geminal bis(phosphonic acid) appended to 1,4,7-triazacyclonone-1,4-diacetic acid fragment through acetamide (NOTAM^{BP}) or methylenephosphinate (NO2AP^{BP}) spacers designed for ^{68}Ga were prepared. Ga^{III} complexation is much faster for ligand with methylenephosphinate spacer than that with acetamide one, in both chemical (high reactant concentrations) and radiolabeling studies with no-carrier-added ^{68}Ga. For both ligands, formation of Ga^{III} complex was slower than that with NOTA owing to the strong *out-of-cage* binding of bis(phosphonate) group. Radiolabeling was efficient and fast only above 60 °C and in a narrow acidity region (pH ~3). At higher temperature, hydrolysis of amide bond of the carboxamide-bis(phosphonate) conjugate was observed during complexation reaction leading to Ga–NOTA complex. *In vitro* sorption studies confirmed effective binding of the ^{68}Ga complexes to hydroxyapatite being comparable with that found for common bis(phosphonate) drugs such as pamindronate. Selective bone uptake was confirmed in healthy rats by biodistribution studies *ex vivo* and by positron emission tomography imaging *in vivo*. Bone uptake was very high, with SUV (standardized uptake value) of 6.19 ± 1.27 for [^{68}Ga]NO2AP^{BP}) at 60 min p.i., which is superior to uptake of ^{68}Ga–DOTA-based bis(phosphonates) and [^{18}F]NaF reported earlier (SUV of 4.63 ± 0.38 and SUV of 4.87 ± 0.32 for [^{68}Ga]DO3AP^{BP} and [^{18}F]NaF, respectively, at 60 min p.i.). Coincidently, accumulation in soft tissue is generally low (e.g. for kidneys SUV of 0.26 ± 0.09 for [^{68}Ga]NO2AP^{BP} at 60 min p.i.), revealing the new ^{68}Ga complexes as ideal tracers for noninvasive, fast and quantitative imaging of calcified tissue and for metastatic lesions using PET or PET/CT. Copyright © 2014 John Wiley & Sons, Ltd.

Additional supporting information may be found in the online version of this article at the publisher's web site.

Keywords: bis(phosphonate); NOTA derivatives; bone targeting; ^{68}Ga radiopharmaceuticals; phosphinate complexes; macrocyclic complexes; PET imaging; radiotracer biodistribution; *in vivo* imaging; nuclear medicine

1. INTRODUCTION

Positron emission tomography (PET) is a powerful method for imaging various tissue or physiological states. The choice of the proper PET radionuclide is given by various criteria such as half-life, energy of the emitted positron, production pathway, radiopharmaceuticals preparation and/or means of application. Compared with the most commonly used radioisotopes (^{11}C and ^{18}F) needing on-site production on a cyclotron, various metal radionuclides can conveniently be prepared utilizing a generator – a device containing a parent nuclide that decays with a long half-life to a daughter positron-emitting radionuclide which is periodically eluted off, purified and used. These radionuclide generators are relatively cheap, permanently accessible and easy to handle. One of the most promising generator-produced radionuclides is ^{68}Ga ($t_{½}$ 67.7 min, 89% positron emission, mean β^+ energy 0.83 MeV) available from commercial ^{68}Ge/^{68}Ga generators (1–7).

However, with only very limited exceptions, most of metal radioisotopes cannot be applied in a 'free' form. The metal radioisotope must be bound in a stable complex to avoid nonspecific deposition of the radioisotope in tissues. Ligands used for complexation of metal ions must ensure very fast and efficient complexation even in highly diluted solutions, sufficient kinetic inertness and thermodynamic stability of the complexes as well as specific accumulation of the formed species in tissue of interest. The last requirement is commonly fulfilled either by creating a metal–ligand system showing specific interaction with target organs or by adding a biologically relevant targeting vector to the metal-ligand system, thereby turning 'normal' ligand into a 'bifunctional' one. Bifunctionality defines utilization of one of functional groups of the ligand to covalent attachment of the ligand to targeting vector while preserving complexing potency of the remaining structure.

Bone tissue is a prominent target of radionuclide diagnostics and therapeutics as bone metastases represent a very common complication of various types of cancer. Generally, bone targeting is mostly realized via attachment of a germinal bis(phosphonate) moiety to a molecule to be delivered to bone (8–11). Bis(phosphonates)

* *Correspondence to: P. Hermann, Department of Inorganic Chemistry, Faculty of Science, Charles University in Prague, Hlavova 2030, 128 43 Prague 2, Czech Republic. E-mail: petrh@natur.cuni.cz*

a *J. Holub, V. Kubíček, P. Hermann*
Department of Inorganic Chemistry, Faculty of Science, Charles University in Prague, Hlavova 2030, 128 43 Prague 2, Czech Republic

b *M. Meckel, F. Rösch*
Institute of Nuclear Chemistry, University Mainz, Fritz-Strassmann-Weg 2, 55128 Mainz, Germany

show a high affinity to hydroxyapatite (HAP). Thus, compounds containing a bis(phosphonate) moiety are efficiently adsorbed on surface of bones. Consequently, such conjugates have been used to deliver radioisotopes to calcified tissues (10). Recently, we and others have developed bis(phosphonate)-bearing ligands based on a DOTA-like macrocyclic core (DOTA = 1,4,7,10-tetraazacyclododecane-1,4,7,10-tetraacetic acid, Fig. 1) as carriers for metal ions to be delivered to calcified tissue (12–17). The applications include imaging techniques (^{111}In and ^{68}Ga for Single-Photon Emission Computed Tomography (SPECT) and Positron Emission Tomography (PET) imaging, respectively) (13,15,17–19) as well as therapy (^{177}Lu, ^{90}Y) (13,16) or bone metastases pain palliation in human patients (20). The conjugates exhibited a very high affinity to HAP as bis(phosphonate) moiety is not coordinated to central metal ion and, thus, remains active for bone targeting (21,22). However, DOTA-like macrocycles are not the best ligands for Ga^{III} as incorporation of the ion inside macrocyclic cavity leads to severe distortion of coordination octahedron around the Ga^{III} ion (23–26).

Despite high thermodynamic stability and kinetic inertness of the Ga^{III} complexes with DOTA-like ligands (27), complexation of no-carrier-added (n.c.a.) ^{68}Ga with these ligands is less efficient and more sensitive to experimental conditions than that of NOTA analogs (NOTA = 1,4,7-triazacyclononane-1,4,7-triacetic acid, Fig. 1) (1). Triaza- instead of tetraazamacrocycles have been proved to be more suitable for Ga^{III} ion. They form complexes exhibiting much higher thermodynamic stability as well as kinetic inertness (28,29). The size of coordination cavity imposed by the nine-member macrocyclic ring corresponds very well to size of Ga^{III} ion. As Ga^{III} is a small ion and mostly requires an octahedral coordination sphere, NOTA-like ligands provide an optimal size and arrangement of ligand cavity to accommodate trivalent gallium ($\log K_{[Ga\text{-}DOTA]} = 26.1$, $\log K_{[Ga\text{–}NOTA]} = 29.6$) (27,28). Thus, a number of NOTA-like ligands have been investigated as promising chelators for ^{68}Ga (1,10). Among them (by analogy with the most commonly used ligands in DOTA-like family, the DOTA-monoamides), NOTA-monoamides appear as an emerging class of ligands owing to their easy synthesis and potential easiness of introduction of bifunctionality through amide formation (30–33).

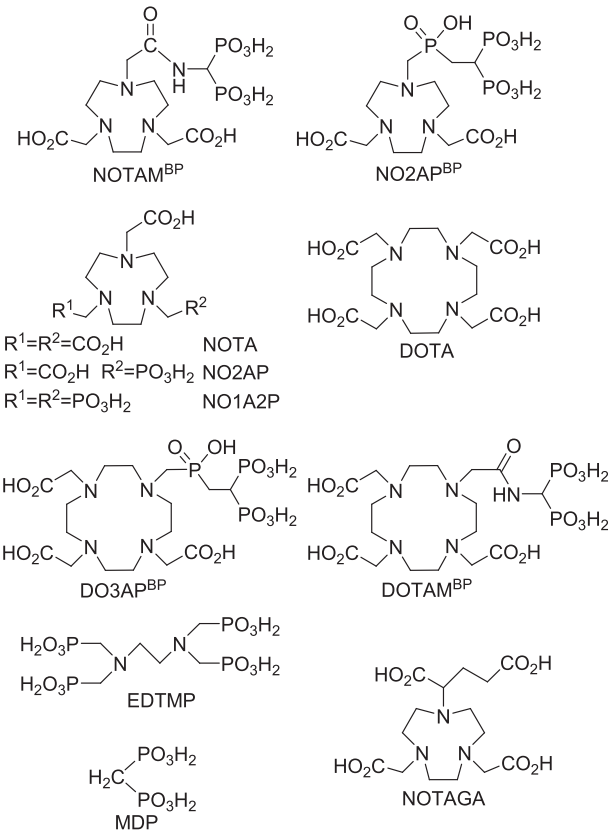

Figure 1. Ligands discussed in this paper.

Imaging of bone lesions is important for the location, staging and treatment of several diseases, mainly breast and prostate cancers metastases. Bone scans have been dominated by SPECT imaging with ^{99m}Tc-bis(phosphonate) tracers. However, SPECT resolution and sensitivity is inferior compared with PET, so PET tracers should be more convenient. [^{18}F]NaF tracer was introduced for bone imaging some time ago. However, ^{18}F is expensive, and its production requires cyclotron and skilled staff. Therefore, cheaper alternative isotopes requiring only relatively simple workup, such as ^{68}Ga produced in a long-lived generator, are desired. We have introduced (12–14) bis(phosphonate)-containing macrocyclic ligands, DOTA-monoamide DOTAM^{BP} and DOTA monophosphinate analog DO3AP^{BP} (Fig. 1), which were successfully labeled with ^{68}Ga and used as PET tracers (18–20,34). However, labeling DOTAM^{BP} and DO3AP^{BP} with ^{68}Ga is not optimal (19,34). Thus, in order to improve the properties of the bone-targeted complexes, such as ease of labeling and improved bone/soft tissue ratio, as well as to get a direct comparison with our previous data on ^{68}Ga-DOTAM^{BP} and ^{68}Ga-DO3AP^{BP}, we decided to study analogous ligands derived from NOTA.

Thus, this paper describes the synthesis of NOTA-like ligands with a bis(phosphonate)-containing side arm (as the bone-targeting group) connected to a metal-binding cage through acetamide or methylphosphinate pendant arms, NOTAM^{BP} and NO2AP^{BP} (Fig. 1). The ligand physicochemical characterization, labeling with ^{68}Ga, *in vitro* binding to HAP, *ex-vivo* biodistribution of the ^{68}Ga-labeled compounds and small animal *in vivo* PET imaging were evaluated. In order to simplify the text, abbreviations such as NOTA, Ga–NOTAM^{BP} and Ga–NO2AP^{BP} are used for the ligands/complexes regardless of the in charge/protonation state, except when the distinction is necessary for comprehension.

2. RESULTS AND DISCUSSION

2.1. Synthesis

The ligands were synthesized according to Fig. 2. A previously described procedure (35) for benzyl monoprotected macrocycle **2** was modified to a one-pot synthesis and its overall yield was improved. Further reaction with *t*-butyl bromoacetate followed by catalytic hydrogenation resulted in doubly substituted macrocycle **4**. Preparations of compound **4**, commonly used for synthesis of 1,4,7-triazacyclononane-1,4-diacetic acid (NO2A) derivatives, have been known for a long time (36–39); however, synthesis here was slightly modified, run on a much higher scale and resulted in overall yield comparable with the previous ones. Secondary amine of NO2A diester **4** was used for attachment of geminal bis(phosphonate) moiety via acetamide or methylphosphinate linkers. The reactions were carried out with fully esterified reagents owing to their better solubility in organic solvents and more efficient chromatographic purification of intermediates. Acetamide derivative **6** was prepared by alkylation of **4** with the appropriate chloroacetamide **5**. Phosphinate derivative **8** was prepared by Mannich-type reaction using paraformaldehyde and per(ethyl) bis(phosphono)-phosphinate **7**. Cleavage of ester

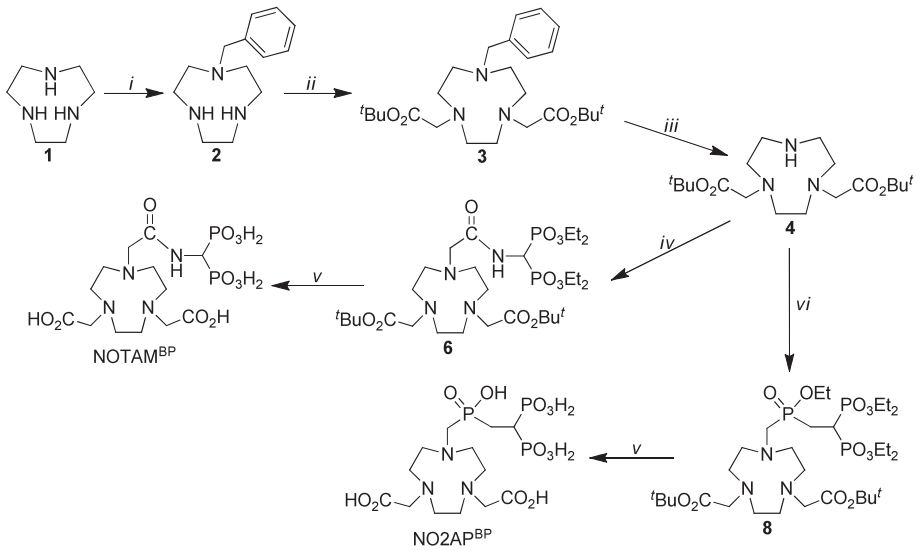

Figure 2. Syntheses of ligands: (*i*) 1, $Me_2NCH(OMe)_2$, dioxan, reflux, 3 h; 2, $BrCH_2Ph$, THF, room temperature (r.t.), overnight; 3, KOH, H_2O/EtOH, reflux, 3 days; 75%. (*ii*) $BrCH_2CO_2{}^tBu$, K_2CO_3, acetonitrile, r.t., 3 days; 91%. (*iii*) H_2, Pd/C, EtOH, 50 °C, 12 h; 84%. (*iv*) $ClCH_2C(O)NH–CH(PO_3Et_2)_2$ (**5**), K_2CO_3, acetonitrile, 50 °C, 3 d; 83%. (*v*) 1. $CF_3CO_2H/CHCl_3$ 1:1, r.t., 12 h; 2. $BrSiMe_3$, acetonitrile, r.t., 12 h; 80% (NOTAM^{BP}), 41% (NO2AP^{BP}). (*vi*) $HP(O)(OEt)CH_2CH(PO_3Et_2)_2$ (**7**), $(CH_2O)_n$, acetonitrile, 35 °C, 3 days; 72%.

protecting groups was performed in two steps. First, *t*-butyl groups were cleaved by action of trifluoroacetic acid and, then, ethyl groups were removed by transesterification with trimethylbromosilane followed by silyl group removal with methanol. The final purification on cation exchange resin yielded NOTAM^{BP} and NO2AP^{BP} in zwitterionic form.

2.2. Ga^{3+} Complexation

Coordination ability of the title ligands toward trivalent gallium was studied owing to their intended applications for ^{68}Ga PET imaging. In addition, Fe^{III} complexes were prepared as this ion shows similar properties (the same charge and similar ionic radius) as the Ga^{III} ion and thus can be considered as a surrogate differing just in spectral and magnetic properties.

Dissolving the ligands in a solution containing equimolar amount of the metal ions leads to significant decrease in pH (pH drops to 1.4–2.0). Addition of strong hydroxide and increase of pH (>2) leads to immediate formation of precipitates. The precipitates are dissolved upon further increase in pH (>4). Most likely, such behavior could be ascribed to a mechanism of complex formation involving several intermediates, as has been suggested for similar macrocyclic ligands (14,28,29). The initial mixing of reagents leads to immediate coordination of the metal ion to bis(phosphonate) oxygen atoms and release of protons. It is known that bis(phosphonate) group is able to interact with trivalent metal ions even at very low pH (40,41) and, at pH < 2, the ligands bind the metal ion in a protonated form (with protons bound on macrocyclic amines as well as on phosphonate groups) forming *out-of-cage* complexes. Such species have overall positive charge and are soluble in water. Increase of pH causes further deprotonation of bis(phosphonate) group and formation of charge-neutral complexes with low solubility in water. Such solid *out-of-cage* intermediates are expected to be 3-D coordination polymers having metal ions bridged by phosphonate group(s), typical for phosphonate and bis(phosphonate) complexes (40,41). Further pH increase results in dissolution of the precipitates and is associated with ring amine deprotonation and formation of final *in-cage* macrocyclic complexes where the metal ion is coordinated with three ring nitrogen atoms and three oxygen atoms of carboxylate or acetamide/phosphinate pendants (29,42,43). A similar mechanism involving a phosphonate-coordinated *out-of-cage* intermediate has been previously postulated for complexation of lanthanide(III) ions with analogous DOTA-like bis(phosphonate)-bearing ligands such as DO3AP^{BP} (12,14). Formation of the *in-cage* complexes was directly confirmed by ^{71}Ga nuclear magnetic resonance (NMR) measurements. The Ga–NO2AP^{BP} complex shows a rather broad signal at 158 ppm ($\varpi_{½}$ ~1300 Hz, Fig. S1 in the Supporting Information). Quadrupole moment of the ^{71}Ga nucleus leads to a signal broadening if Ga^{III} ion is placed in a nonsymmetrical coordination environment. Nonsymmetrical charge distribution leads to an extremely broad signal of Ga–NOTAM^{BP} complex centered at ~170 ppm ($\varpi_{½}$ = ~9700 Hz, Fig. S1); a ^{71}Ga NMR chemical shift of 166 ppm has been observed for other NOTA–monoamide gallium(III) complexes (31).

The time course of gallium(III) complexation with NO2AP^{BP} was studied in details by ^{71}Ga and $^{31}P\{^1H\}$ NMR. Coordination spheres of the *out-of-cage* intermediates are completely nonsymmetrical and, thus, are 'invisible' in ^{71}Ga NMR spectra. Thus, formation of the *in-cage* complex was quantified using an external capillary standard. These experiments were performed with Ga:L 1:1 molar ratio, at pH 2 and 3 (1 M sodium chloroacetate buffer), pH 4 and 5 (1 M sodium acetate buffer). In the presence of weakly coordinating buffers, the above-mentioned precipitation of intermediates was not observed. The results are summarized in Table 1 and Figs. 3 and S2 (in the Supporting Information). Complexation rates follow the order pH 2 < pH 3 ~ pH 5 < pH 4. As stated above, the complexation can be described as a two-step process. The intermediate *out-of-cage* complex is formed instantly and metal ion is coordinated only through oxygen atoms of bis(phosphonate) group and pendant arms (carboxylate and phosphinate), whereas macrocyclic amines are protonated. In the rate-determining step, ring nitrogen atoms lose proton(s) and the metal ion simultaneously moves into the macrocycle cavity; it is generally a base-catalyzed process. The mechanism explains the increase in complexation rate between pH 2 and 3.

Table 1. Half-time ($t_{1/2}$) of Ga–NO2AP^{BP} complex formation (40 °C, molar ratio L:Ga = 1:1, c_{Ga} = 0.13 M)

Ligand	pH	$t_{1/2}$ (min)	95% Complexation (min)
NO2AP^{BP}	5	10	50
	4	<5	20
	3	12	60
	2	65	360
NOTA[a]	3	<2	
	1	270	

[a]25 °C, Šimeček *et al.* (28).

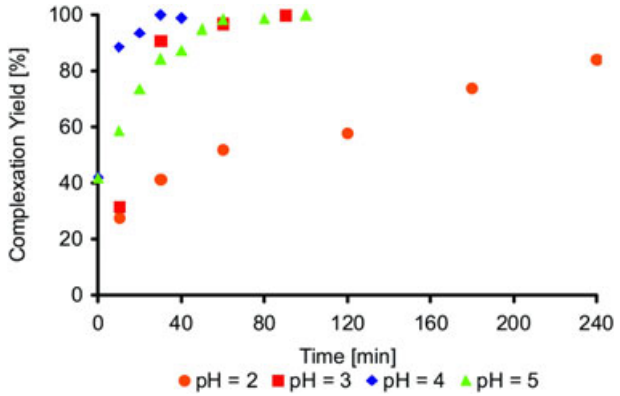

Figure 3. Time course of complexation of Ga^{III} ion with NO2AP^{BP} at different pH (40 °C, molar ratio L:Ga = 1:1, c_{Ga} = 0.13 M); dead time for t_0 = 5 min.

Complexation at pH 5 might be partially decelerated by the presence of acetate anions from the buffer; however, at the milimolar concentrations used in these experiments, partially protonated bis(phosphonate) anion (41) is a much better ligand than acetate and it is known that phosphonate coordination ability is considerably increased with consecutive deprotonation of the group. Thus, slower complexation at pH 5 is probably caused by more extensive deprotonation of bis(phosphonate) moiety at higher pH leading to its stronger interaction with Ga^{III} ion and stabilization of the *out-of-cage* complex, or by formation of Ga^{III} hydroxido complexes.

In the case of NOTAM^{BP}, broadening of the ^{71}Ga NMR signal and overlapping of the ^{31}P{^{1}H} NMR signals of the product and reaction intermediates disabled precise quantification under the same conditions as those used for NO2AP^{BP} complexation. However, even after heating at 40 °C for several hours, broad ^{31}P{^{1}H} NMR signals were observed, showing that only an *out-of-cage* complex was formed which was stable under these conditions. If the solution was heated at 95 °C (Figs. 4 and S3 in the Supporting Information), several signals could be distinguished after several minutes and the spectra indicate that the *in-cage* complex is fully formed after ~30 min under this conditions. Further heating led only to a decrease of Ga–NOTAM^{BP} complex signal and increase of that of aminomethylene-bis(phosphonate), indicating that Ga–NOTAM^{BP} complex is unstable under these conditions and decomposes to Ga–NOTA complex (see also below). Some decomposition {i.e. formation of [Ga(NOTA)]} was observed in ^{71}Ga NMR spectrum even after 10 min of the reaction (Fig. S3).

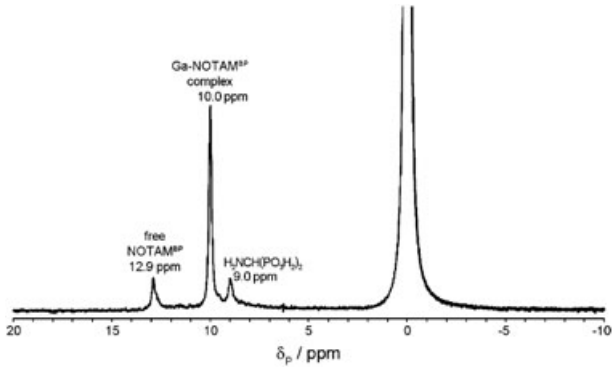

Figure 4. ^{31}P{^{1}H} NMR spectrum of reaction mixture after 30 min of reaction of Ga^{III} ion with NOTAM^{BP} at pH 3 and 90 °C [c_{Ga} = 0.13 M, slight molar excess of ligand; dead time (t_0) ~5 min].

The results point to an important role of spacer connecting bis(phosphonate) group and macrocycle. Under all conditions tested, NO2AP^{BP} showed significantly faster gallium(III) complexation than NOTAM^{BP}. Albeit phosphinates are known to be better complexation groups than carboxamides, the pronounced difference in reaction rate is surprising; a hard and charged phosphinate group as a good coordinating group for Ga(III) ion is probably able to assist ion transfer from the *out-of-cage* species into the *in-cage* complex much better. In addition, the basicity of amine group in N–CH_2–P(R)O_2H moiety is significantly lowered (28,44) and, so, deprotonation of the amine group adjacent to the phosphinate is facilitated.

For both ligands, complexation rates are significantly lower than those reported for NOTA or its phosphinic acid analogs (28,29,45–47). Therefore, the presence of a too strongly complexing hard group such as bis(phosphonate) in proximity to the macrocycle could be considered as a rate-decreasing factor in the Ga^{3+} complexation reaction. In addition, it has recently been reported that the presence of three bis(phosphonate) groups in the side chains of a tris(methylenephosphinic acid) NOTA analog completely prevents the Ga^{III} ion entering into the macrocyclic cavity and the Ga^{III} ion is coordinated only by phosphonate groups in an *out-of-cage* fashion (48). Consequently, a number of bis(phosphonate) groups should be balanced to have good bone targeting and, at the same time, efficient *in-cage* complexation.

2.3. Hydrolysis of the Amide Bond in the Ga–NOTAM^{BP} Complex

Single crystals were formed in the time course of gallium(III) complexation with NOTAM^{BP}. According to the X-ray diffraction, these were not crystals of Ga–NOTAM^{BP} but those of a known Ga–NOTA complex (41). This is result of the amide bond hydrolysis in the Ga–NOTAM^{BP} complex (see also Fig. 5). Upon complexation, the Ga^{III} ion is coordinated through amide oxygen or nitrogen atoms (31). This coordination decreases the electron density on the amide carbon atom and makes it more vulnerable to solvent nucleophilic attack (it is the same effect as that responsible for hydrolysis of peptide bond catalyzed by metalloenzymes).

As the reaction is important in view of utilization of ^{68}Ga-labeled ligands in nuclear medicine (see below), the hydrolysis was studied in more detail. It was monitored through an increasing intensity of sharp Ga–NOTA signal in ^{71}Ga NMR (δ_{Ga} = 170 ppm; $\varpi_{½}$ = 390 Hz) and, in parallel, through increasing intensity of aminomethyl-bis(phosphonate) signal in ^{31}P{^{1}H} NMR (δ = 8.9 ppm,

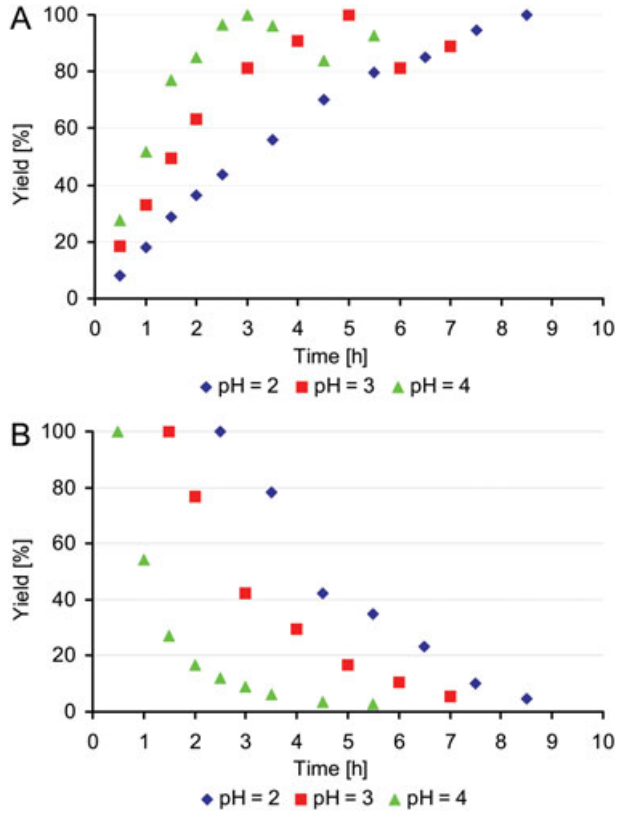

Figure 5. Hydrolysis of amide bond in Ga–NOTAM^{BP} complex expressed as increasing abundance of Ga–NOTA complex in ^{71}Ga NMR (A) and decreasing abundance of Ga–NOTAM^{BP} complex in ^{31}P{^{1}H} NMR (B) (90 °C, c_{GaL} = 0.13 M). Figures do not have the same *y*-axis absolute scale: precipitation of the Ga–NOTA complex, confirmed by X-ray diffraction, caused decline of ^{71}Ga NMR signal intensity by the end of the reaction and maximum in ^{31}P{^{1}H} NMR data refers to a time when the first integration was possible, that is, after 0.5–2.5 h depending on pH.

pH 3), Fig. S3 in the Supporting Information. The results show that the hydrolysis is faster with increasing pH (Fig. 5). This indicates a hydroxide-mediated reaction and could be explained as nucleophilic attack of hydroxide anion on the amide carbon atom of highly polarized carbonyl moiety owing to coordination to a small trivalent metal ion; thus, the reaction can proceed even in slightly acidic solutions. However, the hydrolysis proceeds at a slower rate than formation of the *in-cage* complex as only some decomposition was observed during 10 min at 90 °C (Fig. S3, see also above) under these 'chemical' conditions (in this context, 'chemical' conditions means milimolar or higher concentrations of reactants, unlike 'radiochemical' conditions where concentrations are many orders of magnitude lower). Thus, the hydrolysis was also checked during labeling of NOTAM^{BP} with ^{68}Ga and ^{68}Ga–NOTA complex was also identified via radio-high-performance liquid chromatography (radio-HPLC; see below).

It should be noted that analogous hydrolysis might have been present during studies of Ga^{III} complexes with simple NOTA-monoamides where a very broad ^{71}Ga NMR signal of the complexes with a small sharp singlet at 170 ppm (probably attributable to Ga–NOTA complex) was observed (31).

2.4. Adsorption of Iron(III) Complexes on Hydroxyapatite

To estimate bone targeting efficiency, the most commonly used method is to determine binding ability of the molecules on the HAP surface. For bis(phosphonate)-containing DOTA derivatives, a long-lived ^{160}Tb metal isotope has been used as a surrogate for lanthanide(III) ions (21). As ^{68}Ga is a short-lived radioisotope, another method was sought. Trivalent iron has properties (charge, size, hardness, etc.) similar to those of trivalent gallium and both ions form analogous complexes; thus, Fe^{III} ion was chosen as a surrogate. UV–vis spectroscopy was used to quantify the sorption ability as Fe^{III} complexes exhibit an intensive ligand-to-metal

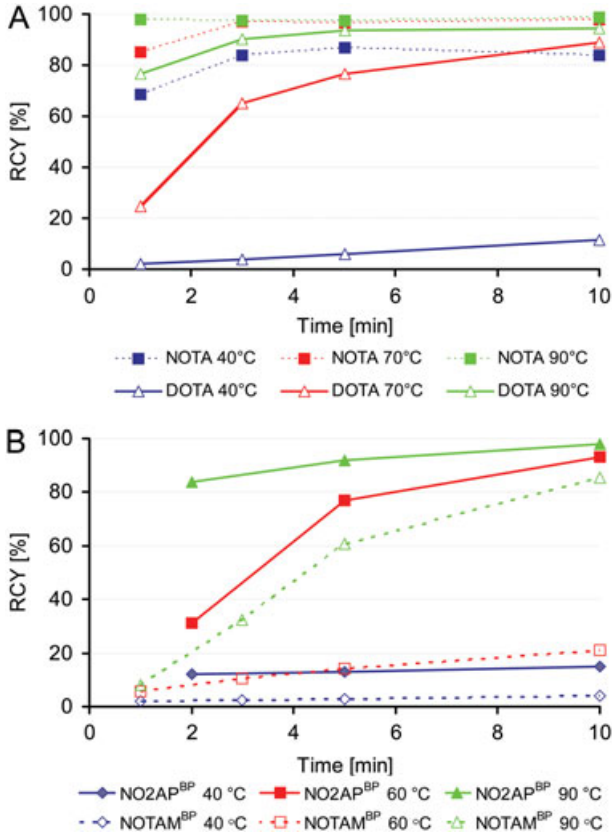

Figure 6. Time course of incorporation of no-carrier-added ^{68}Ga by NOTA and DOTA (A, pH 4.0) and the title ligands (B, pH 4.2) at various temperatures. Results for NOTAM^{BP} can be influenced by amide bond hydrolysis (for details, see text).

Table 2. Adsorption parameters of Fe^{III} complexes on hydroxyapatite surface (pH 7.5, 25 °C, equilibration time 3 days)

	Complex			
Constant	Fe-NOTAM^{BP}	Fe-NO2AP^{BP}	Fe-DOTAM^{BP}	Fe-DO3AP^{BP}
$K/10^3$ (dm^3 mol^{-1})	31.3 ± 6.1	20.0 ± 3.2	43.7 ± 12.2	207.6 ± 45.3
$X_m/10^{-6}$ (mol m^{-2})	1.007 ± 0.035	1.271 ± 0.052	0.768 ± 0.019	1.015 ± 0.017

charge transfer band in UV region (Fig. S4 in the Supporting Information). Iron(III) complexes of DOTAM^{BP} and DO3AP^{BP} were also prepared and studied for comparison with analogous complexes of DOTA-like ligands already used as ^{68}Ga radiopharmaceuticals (19,20).

The adsorption process is usually described by the Langmuir adsorption isotherm:

$$\frac{X}{X_m} = \frac{K \times c}{1 + (K \times c)}$$

where K is the analyte (complex) affinity constant for the surface (in dm^3 mol^{-1}), X_m is the maximum sorption capacity of the complex (in mol m^{-2}), c is the complex concentration (in mol dm^{-3}) in solution and X is the specific adsorbed amount of the complex (in mol m^{-2}). Aqueous suspension of HAP was used as a model of bone tissue. The results are shown in Fig. S5 in the Supporting Information and the absorption parameters are summarized in Table 2.

All complexes studied show efficient binding on HAP surface. Maximum sorption capacities are in a range that corresponds to formation of monomolecular layer (12). For complexes of NOTA analogs, maximum sorption capacities are higher than those for DOTA complexes. This could be explained by compact shape of Fe^{III} complexes with NOTA derivatives, where all pendant arms are coordinated (49,50). The larger size of the cyclen ring and the presence of two uncoordinated pendant arms in complexes with DOTA-like ligands (51) result in a larger surface area occupied by one molecule of DOTA complexes. Higher affinity constants found for complexes with DOTA derivatives indicate that uncoordinated pendant arms might be involved in interaction with HAP surface; the higher affinity constant for Fe^{III}-DO3AP^{BP} complex can be probably explained by the highest overall charge among the complexes. Generally, both affinity constants as well as sorption capacities are comparable to those previously reported for lanthanide(III) complexes with the same DOTA analogs, where all pendant arms are bound to central metal ion (e.g. $K = 250 \times 10^{-3}$ dm^3 mol^{-1} and $X_m = 0.65 \times 10^6$ mol m^{-2} for ^{160}Tb-DO3AP^{BP} complex) (21) as well as to those for simple bis(phosphonates), for example, for pamidronate ($K = 44 \times 10^{-3}$ dm^3 mol^{-1} and $X_m = 1.82 \times 10^6$ mol m^{-2}) (21). This indirectly confirms similar accessibility of distant bis(phosphonate) moiety for bone targeting in all complexes.

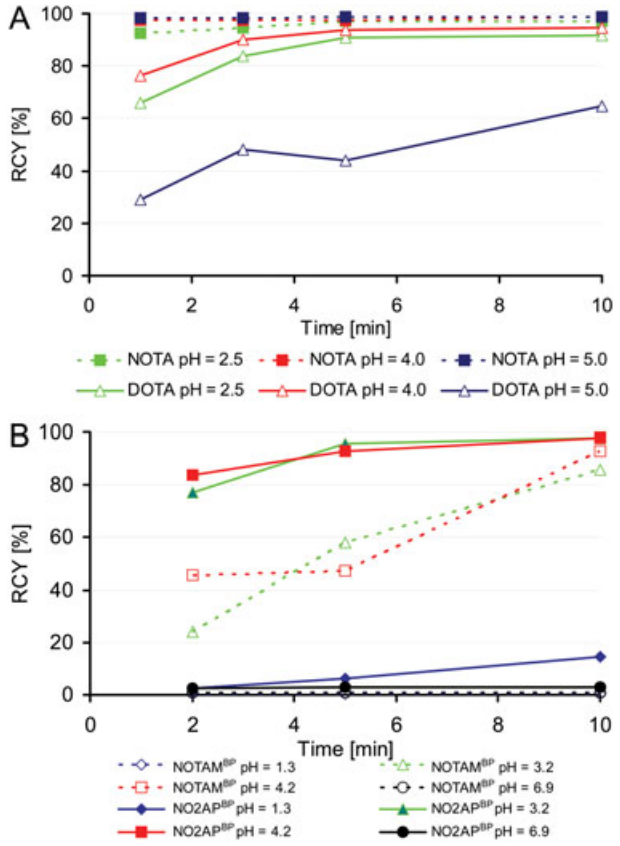

Figure 7. Time course of incorporation of no-carrier-added ^{68}Ga by NOTA and DOTA (A) and the title ligands (B) at 95 °C and various pH. Results for NOTAM^{BP} can be influenced by amide bond hydrolysis (for details, see text).

2.5. Radiolabeling With No-carrier-added ^{68}Ga

If ligands are considered as potential radiopharmaceuticals, the efficiency of metal radionuclide incorporation is one of their most important properties and, thus, the title ligands were

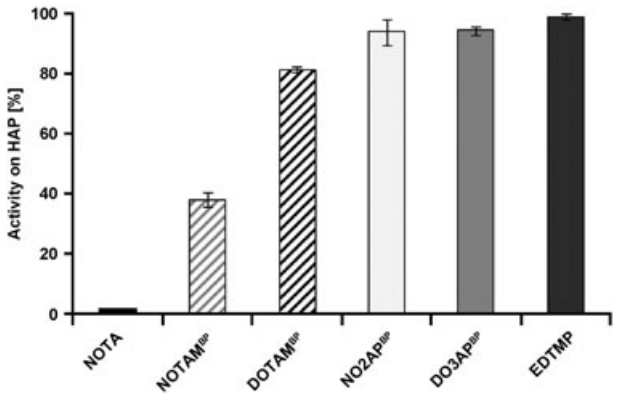

Figure 8. Binding of ^{68}Ga-labeled complexes to hydroxoapatite in isotonic saline (room temperature, 10 min). Data for [^{68}Ga]DOTAM^{BP} (19) and [^{68}Ga]EDTMP (53) were taken from literature (for EDTMP formula, see Fig. 1). Results for NOTAM^{BP} can be influenced by amide bond hydrolysis (for details, see text).

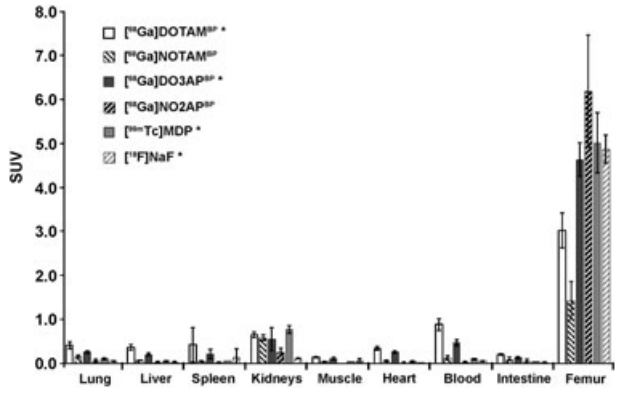

Figure 9. Biodistribution data for different bone-binding ^{68}Ga radiotracers and [^{18}F]NaF in healthy male Wistar rats ($n = 5$) after 60 min. p.i. *Data for [^{68}Ga]DOTAM^{BP}, [^{68}Ga]DO3AP^{BP}, [^{18}F]NaF and [^{99m}Tc]MDP (for MDP formula, see Fig. 1) were taken from the literature (19,34). Results for NOTAM^{BP} can be influenced by amide bond hydrolysis (for details, see text).

Table 3. *Ex vivo* biodistribution of [^{68}Ga]NOTAM^{BP} and [^{68}Ga]NO3AP^{BP} complexes in healthy male Wistar rats (60 min p.i.). Data are presented as an average from five animals (±SD); uptake as percentage injected dose per gram of tissue

Complex	Organ									
	Lung	Liver	Spleen	Kidney	Muscle	Heart	Blood	Intestime	Testes	Femur
[^{68}Ga]NOTAM^{BP}	0.12 ± 0.03	0.05 ± 0.01	0.04 ± 0.01	0.45 ± 0.04	0.03 ± 0.01	0.04 ± 0.01	0.09 ± 0.04	0.07 ± 0.03	0.04 ± 0.01	1.12 ± 0.36
[^{68}Ga]NO2AP^{BP}	0.04 ± 0.03	0.02 ± 0.01	0.02 ± 0.01	0.18 ± 0.07	0.01 ± 0.00	0.01 ± 0.01	0.02 ± 0.00	0.03 ± 0.03	0.01 ± 0.00	4.37 ± 0.92

tested by labeling with n.c.a ^{68}Ga. The ligand-to-^{68}Ga^{III} molar ratio was approximated in the order of 10^4 in all experiments (1 MBq ^{68}Ga corresponds to ~0.01 pmol of Ga^{III}). Complexation was followed [see an example of thin-layer chromatography (TLC) plate in electrospray ionization (ESI), Fig. S6 in the Supporting Information] at various temperatures and solution acidities, and the results are summarized in Figs. 6 and 7.

The data show similar trends to those obtained in NMR experiments (above). For both ligands, fast complexation requires weakly acidic conditions, that is, pH 3–4. No complexation was observed at pH 1.3 and 6.9 at any temperature. The experiments also confirmed strong dependence of complexation rate on temperature. At pH 4.2 and at room temperature, no complexation was observed with both ligands. In the case of NO2AP^{BP}, heating to 60 °C is required to reach full complexation in 10 min; at 95 °C, ^{68}Ga^{III} was quantitatively bound in only 5 min. Temperatures of $<$60 °C were insufficient for radiolabeling with NOTAM^{BP} and reasonable complexation efficiency was reached only at a temperature of 95 °C. However, radio-TLC cannot be used for evaluation of hydrolysis of amide bond in ^{68}Ga–NOTAM^{BP} system (as observed in NMR experiments, above) as all complexes have the same mobility. To check the decomposition, labeling of NOTAM^{BP} was carried out under conditions used in sample preparation for *in-vivo* experiments (pH 4.5, 95 °C, 15 min) and the reaction mixture was evaluated by HPLC on amine-containing sorbent (Fig. S7 in the Supporting Information). Partial decomposition (~20%) was observed while ^{68}Ga–NOTAM^{BP} complex was fully formed during the time; therefore, amide bond hydrolysis is slower than ^{68}Ga^{III} complexation under these conditions. The partial hydrolysis probably influenced sorption and *in-vivo* data (see below). NO2AP^{BP} showed much faster complexation of n.c.a. ^{68}Ga^{III} than NOTAM^{BP} under all tested conditions (Figs. 6 and 7). This efficient complexation is more pronounced if compared with ^{68}Ga^{III} labeling of DO3AP^{BP} where radiochemical yield under more forced conditions was, at the best, ~60% (34). It has also been shown (under the same conditions) that the presence of one or two methylphosphonate arms in NOTA analogs (NO2AP and NO1A2P; for formulae, see Fig. 1) accelerates the labeling reaction in comparison with labeling with NOTA (53). Thus, the presence of methylenephosphonic/inic acid pendant arms seems to increase the complexation rate. Radiolabeling of the title ligands with n.c.a. ^{68}Ga is less efficient than that of NOTA; however,

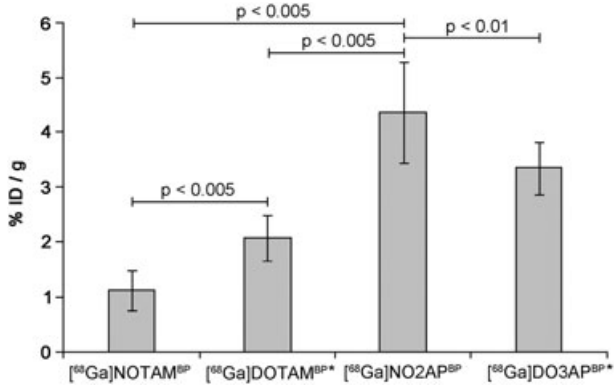

Figure 10. Radioactivity accumulation on femur for [^{68}Ga]NOTAM^{BP}, [^{68}Ga]DOTAM^{BP}, [^{68}Ga]NO2AP^{BP} and [^{68}Ga]DO3AP^{BP} (60 min p.i.). *Data for [^{68}Ga]DOTAM^{BP} and [^{68}Ga]DO3AP^{BP} were taken from the literature (19,34). Results for NOTAM^{BP} can be influenced by amide bond hydrolysis (for details, see text).

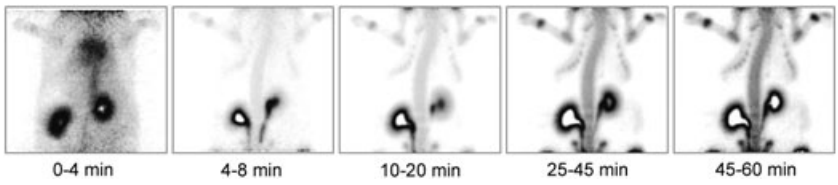

Figure 11. MicroPET image of the second healthy male Wistar rat at different times after injection of 31 MBq [^{68}Ga]NO2AP^{BP}.

NO2AP^{BP} incorporates $^{68}Ga^{III}$ similarly to unsubstituted DOTA (Figs. 6 and 7). Both title ligands are more efficient chelators than DOTAM^{BP} (it needs 20–25 min at 95 °C for 95% labeling and the best pH is ~5; the other labeling conditions are the same as for the title ligands) (19). ^{68}Ga-DOTAM^{BP} complex has been already applied *in vivo* (19,20) and, compared with it, ^{68}Ga-complexes of the title ligands appear better suited for straightforward labeling adequate for utilization *in vivo* (see below).

2.6. Adsorption of ^{68}Ga-labeled Complexes to Hydroxoapatite

Binding of complexes labeled with ^{68}Ga to HAP surface was measured at room temperature (Fig. 8). [^{68}Ga]NO2AP^{BP} complex (93.8 ± 4.4%) is bound much better compared with [^{68}Ga]NOTAM^{BP} complex (38.1 ± 2.6%), while binding of [^{68}Ga]NOTA complex (1.5 ± 0.3%) is negligible under the same conditions. These results do not fully parallel those of iron(III) complexes obtained under 'chemical' equilibrium conditions where no significant differences were observed. [^{68}Ga]NOTAM^{BP} might be partially decomposed during complexation decreasing absorption on HAP. However, the difference is significant and another reason should be present. Because of the short half-life of ^{68}Ga, a short contact time of the complexes with HAP had to be used and full equilibrium could not be reached, unlike during measurements with Fe^{III} complexes (above). Thus, difference between the experiments might be attributed to faster absorption kinetics of [^{68}Ga]NO2AP^{BP} complex if compared with [^{68}Ga]NOTAM^{BP} complex; it was observed that [^{160}Tb]DO3AP^{BP} complex adsorbs on the HAP surface very quickly (22). These results are more relevant for *in vivo* conditions. Compounds with slow adsorption kinetics are not suitable for future *in vivo* studies. It is necessary to obtain high binding to targeted tissue for imaging agents in a short timescale; otherwise long measurement time and high activities are required to develop adequate PET images. However, this experiment showed (Fig. 1) no significant difference in HAP adsorption between [^{68}Ga]NO2AP^{BP}, [^{68}Ga]DO3AP^{BP} and [^{68}Ga]EDTMP tracers [EDTMP = ethylenediamine-*N,N,N′,N′*-tetrakis(methylenephosphonic acid), Fig. 1]. [^{68}Ga]NO2AP^{BP} had a binding of 93.8 ± 4.4% on HAP after 10 min, which is one of the highest rates among ^{68}Ga-labeled macrocyclic bis(phosphonates) (Fig. 9). Data in this experiment correlate well with those of bone accumulation *in vivo* (in *ex vivo* organ distribution, see below).

2.7. *In Vivo* Biodistribution Studies

Uptake of the tracers in organism was followed by both microPET and organ dissection. The dissection data (Table 3) clearly shows high uptake of [^{68}Ga]NO2AP^{BP} in bone (femur 4.37%, 60 min p.i.) and very low uptake in nontarget organs like soft tissues. Similar results have been observed with [^{68}Ga]DOTA-based bis(phosphonates) in published studies (19,34). Bone uptake of [^{68}Ga]NO2AP^{BP} [standardized uptake value (SUV) of 6.19 ± 1.27% injected dose per gram in femur] is clearly superior if compared with the established SPECT, ^{99m}Tc-MDP [MDP = methylene-bis(phosphonic acid), Fig. 1], or PET, [^{18}F]NaF, bone tracers and also higher than that of DOTA-based tracer (Fig. 9). Lower uptake of [^{68}Ga]NOTAM^{BP} is in line with the *in vitro* results and can be caused by partial decomposition during labeling (above). Bone uptake of [^{68}Ga]NO2AP^{BP} is significantly better (Fig. 10) than bone uptake of [^{68}Ga]DOTAM^{BP}, a tracer already successfully used in patients, as well as that of its equivalent DOTA-based tracer, [^{68}Ga]DO3AP^{BP} (19,34). Differences between *ex-vivo* biodistributions and microPET images (below) might be given by a different age of the animals (see Experimental).

To illustrate the usefulness of [^{68}Ga]NO2AP^{BP} as PET tracer, its biodistribution was followed by microPET with two animals. Uptake on bone was observed within a few minutes and labeled compounds were cleared out of the blood during 60–120 min via kidneys and bladder. MicroPET images (Fig. 11) show a rapid clearance of the compound from blood. After 5–10 min, only 10–15% of the injected radiotracer was found in bloodstream, while a very fast accumulation in skeleton was observed. Bone images of good quality can be developed at early time points. In Figs. 11 and S8 (in the Supporting Information), the skeleton is clearly highlighted after only 15 min p.i. In the second animal (Fig. 11), the kidneys show a high uptake as the main clearance organ of [^{68}Ga]NO2AP^{BP} as expressed by SUV values in Figs S9 and S10 in the Supporting Information. After a rapid initial accumulation (up to 50 min. p.i.), the labeled compound is predominantly cleared to bladder and washed out of the animal via urine. [^{68}Ga]NO2AP^{BP} showed a similar kinetics in both animals with only small differences that could be explained by variation in the animals' weight and age. At 60 min p.i., the SUV in spine was 1.8 for animal no. 1 (536 g, 32 MBq) and 1.6 for animal no. 2 (346 g, 31 MBq). Uptake of ^{68}Ga-bis(phosphonate) in bone joints was almost 50% higher (for animal no. 1, SUV in joint of scapula and humerus was 3.1).

3. CONCLUSIONS

New bis(phosphonate)-containing derivatives of NOTA were prepared by scaleable synthesis. They showed efficient complexation of trivalent gallium and phosphinate derivative was shown to bind metal ion better than acetamide derivative under any conditions used. Complexation rates of these new ligands were lower than those of NOTA or its phosphinic acid analogs owing to the presence of phosphonate groups forming a rather stable *out-of-cage* complex which is able to compete with the formation of *in-cage* complex. The amide group in the *in-cage* complex is not fully hydrolytically stable owing to a strong polarizing effect of the small Ga^{3+} ion after its coordination; thus, ^{68}Ga–NOTAM^{BP} cannot be used in practice. These results indicate that complexes of NOTA-amides can be hydrolytically

unstable, unlike complexes of DOTA-amides where analogous hydrolysis has not been observed. The hydrolysis takes place only at high temperature but occurs also during labeling with n.c.a. ^{68}Ga; however, hydrolysis is slower than complexation. This should be taken into account when designing new ligands for Ga^{III} and other highly charged metal ions. Thus, if a NOTA-like skeleton with triacetate pendant arms is required, a ligand not modified on the coordinating acetate group(s) should be considered, for example, NOTAGA derivatives with a distant carboxylic acid group for the chelator conjugation could be a good solution, avoiding the hydrolysis problem.

Radiolabeling with ^{68}Ga was rapid at temperatures above 60 °C for the phosphinate and at 90 °C for the acetamide ligand. Biodistribution and microPET studies in healthy male rats showed very quick uptake of ^{68}Ga-labeled probes on bones and rapid elimination of nontargeted probes through kidneys. The pharmacokinetics of the new labeled macrocyclic ligands is similar to that of labeled DOTA-bis(phosphonate) conjugates as well as that of commonly used ^{99m}Tc-bis(phosphonate) radiopharmaceuticals or [^{18}F]NaF, but results in a significantly higher accumulation of [^{68}Ga]NO2AP^{BP} on bone. [^{68}Ga]NO2AP^{BP} showed a superior adsorption kinetics compared with that of other ^{68}Ga-labeled macrocyclic bis(phosphonates) and a similar affinity HAP to [^{68}Ga]EDTMP; however, [^{68}Ga]EDTMP was reported to be an inefficient radiotracer based on its low kinetic and thermodynamic *in vivo* stability (51). Additionally, the new ligands performed in an almost quantitative labeling (RCY more than 98%) within 10 to 15 min with NO2AP^{BP} being labeled more effectively, while DOTA-based bis(phosphonates) showed an RCY between 70 and 85% and purification steps are necessary before application. For routine synthesis in nuclear medicine practice, easy labeling processes and high RCY are essential. These properties and convenient availability of ^{68}Ga from commercial generators render NO2AP^{BP} as one of the best leading compounds for the development of bone-targeted PET probes.

These new ^{68}Ga-based radiotracers bring improvement of a current state-of-art for bone imaging owing to much better resolution and sensitivity of PET if compared with SPECT and a much lower price of generator-produced ^{68}Ga radioisotope if compared with cyclotron-produced ^{18}F. Despite no ^{68}Ge/^{68}Ga generator having been approved, easy operation of these generators and its continuously decreasing prices make ^{68}Ga-PET based bone scans possibly the most easily implemented PET modality in less developed countries without expensive cyclotrons and skilled staff. Experiments focused on better understanding of biological fate and, finally, directed to a human application of the new probe are under way.

4. EXPERIMENTAL

4.1. General Methods

Reagents **5** and **7**, and ligands DOTAM^{BP} and DO3AP^{BP}, were synthesized according to published procedures (12,14). 1,4,7-Triazacyclononane (tacn) as free base was purchased from CheMatech (France). The other reactants and solvents were commercially available analytical-grade chemicals. Acetonitrile was dried by distillation from P_2O_5. NMR spectra were recorded using Varian Unity Inova (400 MHz), Varian VNMRS (300 MHz) or Bruker Avance (600 MHz) spectrometers. ^{1}H and ^{13}C (at 300 or 600 and 75 or 151 MHz, respectively) NMR shifts were referenced to internal tetramethylsilane or *t*-BuOH signal, the ^{31}P (121 MHz) and ^{71}Ga (129 MHz) NMR shifts were externally referenced relative to 85% aq. H_3PO_4 and 0.1 M aq. $Ga(NO_3)_3$, respectively. Homo- and heteronuclear 2D-NMR spectra were used for final characterization of the title ligands. Mass spectra were recorded on a Bruker Esquire 3000 spectrometer with ESI as ion source and ion trap as a detector in positive or negative modes. UV–vis spectra were recorded using Biochrom Lightwave 2 spectrometer. Elemental analyses were performed using an Haraeus Varian EL III system. TLC analyses of the ligand and intermediates during their synthesis were carried out with silica on aluminum foil (Merck). Radio-TLC analysis was developed with a Canberra Packard Instant Imager. Radioactivity of samples was measured with an Aktivimeter Isomed 2010, MED (Nuklear-Medizintechnik Dresden GmbH). For small animal PET studies, a Siemens microPET Focus 120 was used and data were reconstructed with the Pmod software (PMOD Technologies Ltd). Radioactivity in tissue samples was determined using a Wallac Wizard2 automatic gamma counter (Perkin Elmer, Germany).

4.2. Synthesis of 1-benzyl-1,4,7-triazacyclononane (2)

1,4,7-Triazacyclononane (5.0 g, 39.9 mmol) was dissolved in mixture of 1,4-dioxane (50 ml) and $Me_2NCH(OMe)_2$ (5.52 g, 47.9 mmol). The mixture was refluxed for 3 h, volatiles were evaporated and the residue was re-dissolved in tetrahydrofurane (THF) (40 ml). A solution of benzylbromide (8.6 g, 47.9 mmol) in THF (40 ml) was added slowly under vigorous stirring and a yellow precipitate was formed. Then more THF (30 ml) was added and the mixture was stirred overnight. The yellow powder was filtered off and dissolved in a mixture of water (25 ml), EtOH (50 ml) and KOH (12.5 g). The mixture was refluxed for 3 days. Volatiles were evaporated under reduced pressure, the residue was dissolved in water (20 ml) and the solution was extracted with chloroform (3× 40 ml). The organic fractions containing the product were combined, dried with Na_2SO_4 and solvent was evaporated. The residue was dissolved in aq. HCl (6 M, 20 ml) and the solution was evaporated to dryness. The crude hydrochloride was dissolved in water (10 ml) and crystallized by addition of Et_2O (100 ml). The product was filtered off and dried under vacuum to yield white crystals of **2**·2HCl·H_2O (8.5 g, 75%). NMR (D_2O): ^{1}H δ = 3.07 (CH_2–NBn, 4H, t, $^3J_{HH}$ 6.0 Hz); 3.25 (CH_2–CH_2NBn), 4H, t, $^3J_{HH}$ 6.0 Hz; 3.65 (NH–CH_2CH_2–NH, 4H, s); 3.95 (N–CH_2–C$_{ar}$, 2H, s); 7.47 (aryl H, 5H, bm); ^{13}C{^{1}H} δ = 44.8 (CH_2–CH_2NBn, s); 46.1 (NH–CH_2CH_2–NH, s); 50.2 (CH_2–NBn, s); 61.6 (N–CH_2–C, s); 130.9, 131.4, 132.8, 137.8 (aryl *C*, 4× s). MS(+): 219.9 $[M+H]^+$. Elemental analysis: found (calcd for $C_{13}H_{21}N_3$·2HCl·H_2O) C 51.1 (50.3); H 8.4 (8.1); N 13.4 (13.5).

4.3. Synthesis of Bis(*t*-butyl) 7-benzyl-1,4,7-triazacyclononane-1,4-diacetate (3)

Protected macrocycle **2** (3.0 g, 9.7 mmol) was dissolved in mixture of dry acetonitrile (100 ml) and K_2CO_3 (5.17 g, 38.8 mmol). A solution of *t*-butyl bromoacetate (3.96 g, 20.4 mmol) in dry acetonitrile (150 ml) was slowly added. The reaction mixture was stirred at room temperature for 3 days, then filtered and evaporated. The product was purified by column chromatography (silica gel, EtOH–25% aq. ammonia 20:1). Fractions containing product were combined and evaporated to yield product **3** (4.2 g, 91%) in the form of yellowish viscous oil. NMR ($CDCl_3$): ^{1}H δ = 1.40 [C(CH_3)$_3$, 18H, s]; 2.73, 3.10, 3.50, 3.70 (N–CH_2CH_2–N, 6H + 2H + 2H + 2H; 4 × bm); 3.28 (N–CH_2–CO_2, 4H, s); 4.49

(N–CH_2–C_{ar}, 2H, s); 7.34 + 7.66 (aryl H, 3H + 2H, 2 × m); $^{13}C\{^1H\}$ δ = 30.3 [C(CH_3)$_3$, s]; 51.9 + 53.7 + 55.1 (ring C, 3 × s); 60.3 (N–CH_2–CO_2, s); 61.6 (N–CH_2–C, s); 83.9 [C(CH_3)$_3$, s]; 131.3, 131.7, 133.0 (aryl C, 3 × s); 172.8 (CO_2, 2C, s). MS(+): 448.1 $[M+H]^+$.

4.4. Bis(*t*-butyl) 1,4,7-triazacyclononane-1,4-diacetate (4)

Compound **3** (2.1 g, 4.7 mmol) was dissolved in dry ethanol (175 ml). Pd/C catalyst (400 mg) was added and the reaction mixture was stirred overnight at 50 °C under hydrogen atmosphere (atmospheric pressure). Suspension was filtered and the filtrate evaporated to dryness. The crude product was purified by column chromatography (silica gel, EtOH–25% aq. ammonia 10:1 to elute impurities and 3:2 to eluate product). The product-containing fractions were combined, evaporated and the residue was co-distilled three times with ethanol to remove traces of ammonia to yield colorless viscous oil that solidified after cooling to room temperature (1.41 g, 84%). NMR ($CDCl_3$): ^1H δ = 1.41 [C(CH_3)$_3$, 18H, s]; 2.81 [N(ac)–CH_2CH_2–N(ac), 4H, s]; 3.08 [N(ac)–CH_2CH_2–NH, 4H, bm]; 3.23 [N(ac)–CH_2CH_2–NH, 4H, bm]; 3.39 (N–CH_2–CO_2, 4H, s); $^{13}C\{^1H\}$ δ = 20.1 [C(CH_3)$_3$, s]; 44.5 [N(ac)–CH_2CH_2–NH, s]; 49.0 [N(ac)–CH_2CH_2–NH, s]; 51.7 [N(ac)–CH_2CH_2–N(ac), s] 56.7 (N–CH_2–CO_2, s); 81.9 [C(CH_3)$_3$, s]; 170.7 (CO_2, s). MS(+): 358.0 $[M+H]^+$.

4.5. NOTAM^{BP} in Ester Form (6)

Ester **4** (1.30 g, 3.6 mmol) was dissolved in mixture of dry acetonitrile (75 ml) and annealed K_2CO_3 (2.60 g). Then, a solution of chloroacetamide **5** (2.07 g, 5.4 mmol) in acetonitrile (75 ml) was added. The reaction mixture was stirred at 50 °C for 3 days. Solids were filtered off, filtrate was evaporated and the crude product was purified by column chromatography (silica gel, EtOH to elute impurities, EtOH–25% aq. NH_3 50:1 to elute product). Pure product was obtained as yellowish viscous oil (2.1 g, 83%). NMR ($CDCl_3$): ^1H δ = 1.28 (P–OCH_2CH_3, 12H, t, $^3J_{HH}$ 7.2 Hz); 1.39 [C(CH_3)$_3$, 18H, s]; 2.71 [$N_{(ac)}$–CH_2CH_2–$N_{(ac)}$, 4H, bm]; 2.84 [$N_{(ac)}$–CH_2CH_2–$N_{(am)}$, 8H, s]; 3.29 (NCH_2CONH, 2H, s); 3.35 (NCH_2CO_2, 4H, s); 4.14 (P–OCH_2CH_3, 8H, m); 5.06 (NH–CH–P, 1H, td, $^2J_{PH}$ 21.2 Hz, $^3J_{HH}$ 7.5 Hz); 8.90 (NH, 1H, d, $^3J_{HH}$ 6 Hz);$^{13}C\{^1H\}$ δ = 16.3 (P–OCH_2CH_3, s); 28.1 [C(CH_3)$_3$, s]; 43.6 (NH–CH–P, t, $^1J_{PC}$ 148 Hz); 55.3 [$N_{(ac)}$–CH_2CH_2–$N_{(ac)}$, s]; 56.3 [$N_{(ac)}$–CH_2CH_2–$N_{(am)}$, s]; 59.2 (N–CH_2–CO_2, s); 60.9 (N–CH_2–CO_2, s); 63.2 (P–OCH_2CH_3, d, $^2J_{PC}$ = 10.0 Hz); 80.7 [C(CH_3)$_3$, s]; 171.7 (CO_2, s); 172.2 (CO, s); $^{31}P\{^1H\}$ δ (ppm) 17.2 (s); ^{31}P δ = 17.2 (d, $^2J_{PH}$ 21.2 Hz); MS(+): 701.4 $[M+H]^+$.

4.6. NOTAM^{BP}

Ester **6** (2.1 g, 3.0 mmol) was dissolved in the mixture of $CHCl_3$ (50 ml) and CF_3CO_2H (50 ml) and stirred in the dark at room temperature overnight. Volatiles were evaporated under vacuum and the residue was repeatedly dissolved in CH_2Cl_2 and evaporated. The resulting oil was dissolved in dry acetonitrile (100 ml) and $BrSiMe_3$ (9.8 ml, 60.0 mmol) was added. The mixture was stirred in dark at room temperature overnight. Volatiles were evaporated, and the residue was re-dissolved in acetonitrile and evaporated, and then dissolved in 50% aq. MeOH and evaporated. The residue was dissolved in H_2O (10 ml) and EtOH (100 ml) was added. Crystallization was finished standing in the refrigerator overnight. Product was filtered off and dried under vacuum to yield white powder (1.15 g, 80%). NMR (D_2O, pD 2.9): ^1H δ = 3.34 [$N_{(ac)}$–CH_2CH_2–$N_{(am)}$, 4H, s]; 3.38 [$N_{(ac)}$–CH_2CH_2–$N_{(am)}$, 4H, s]; 3.46 [$N_{(ac)}$–CH_2CH_2–$N_{(ac)}$, 4H, s]; 3.89 (N–CH_2–CO_2, 4H, s); 3.94 (N–CH_2–CO–NH, 2H, s); 4.51 (NH–CH–P, t, $^2J_{PH}$ 24.0 Hz); $^{13}C\{^1H\}$ δ = 47.8 (NH–CH–P, t, $^1J_{PC}$ 125.6 Hz); 50.3 [$N_{(ac)}$–CH_2CH_2–$N_{(ac)}$, s]; 50.5 [$N_{(ac)}$–CH_2CH_2–$N_{(am)}$, s]; 50.7 [$N_{(ac)}$–CH_2CH_2–$N_{(am)}$, s]; 57.5 (N–CH_2–CO_2, s); 57.9 (N–CH_2–CO–NH, s); 169.2 (CO–NH, s); 172.5 (CO_2, s); $^{31}P\{^1H\}$ δ (ppm) 12.7 (s); ^{31}P δ = 12.7 (CH–P, d, $^2J_{HP}$ 24.0 Hz). MS(−): 474.8 $[M-H]^-$. Elemental analysis: found (calcd for $C_{13}H_{26}N_4P_2O_{11}\cdot 1.5H_2O\cdot 0.4HCl$) C 30.0 (30.1); H 5.3 (5.7); N 10.4 (10.8).

4.7. NO2AP^{BP} In Ester Form (8)

Ester **4** (1.55 g, 4.3 mmol) was dissolved in mixture of dry acetonitrile (40 ml) and paraformaldehyde (156 mg, 5.2 mmol). Solution of phosphinate **7** (2.05 g, 5.2 mmol) in acetonitrile (30 ml) was added and the mixture was stirred at 35 °C for 3 days. Volatiles were evaporated and the crude product was purified by column chromatography (silica gel, EtOH to elute impurities, EtOH–25% aq. ammonia 50:1 to eluate the product). The product-containing fractions were combined and evaporated to yield yellowish oil (2.40 g, 72%). NMR ($CDCl_3$): ^1H δ = 1.31 (P–OCH_2CH_3, 15H, m); 1.46 (C(CH_3)$_3$, 18H, s); 2.00–2.80 (PCH_2, PCH, 5H, m); 2.90–3.20 (ring H, 12H, m); 3.56 (N–CH_2–CO_2, 4H, s); 4.18 (P–OCH_2CH_3, 10H, m); $^{13}C\{^1H\}$ δ = 20.5 (CH–P–O–CH_2–CH_3, s); 26.2 (PCH_2CHP, d, $^1J_{PC}$ 82.9 Hz); 32.3 [C(CH_3)$_3$, s]; 34.1 (PCH_2CHP, td, $^1J_{PC}$ 132.1 Hz, $^2J_{PC}$ 26.9 Hz); 58.8, 59.2, 60.6 (N–CH_2CH_2–N, ring C, 3× s); 62.1 (N–CH_2–CO_2, s) 64.1 (NCH_2P, d, $^1J_{PC}$ 95.1 Hz); 67.0 (P–OCH_2CH_3, s); 85.1 [C(CH_3)$_3$, s]; 174.9 (CO_2, s) $^{31}P\{^1H\}$ δ = 22.7 (PCH_2CHP, 2P, d, $^3J_{PP}$ 20.8 Hz); 49.2 ($P$$CH_2$CHP, 1P, t, $^3J_{PP}$ 20.8 Hz). MS(+): 764.4 $[M+H]^+$.

4.8. NO2AP^{BP}

Ester **8** (2.40 g, 3.1 mmol) was dissolved in the mixture of $CHCl_3$ (50 ml) and CF_3CO_2H (50 ml) and stirred in dark at room temperature overnight. Volatiles were evaporated under vacuum and the residue was repeatedly dissolved in CH_2Cl_2 and evaporated. The resulting oil was dissolved in dry acetonitrile (100 ml) and $BrSiMe_3$ (9.8 ml, 60.0 mmol) was added. The mixture was stirred in dark at room temperature overnight. Volatiles were evaporated and the residue was re-dissolved in acetonitrile and evaporated, and then dissolved in 50% aq. MeOH and evaporated. Crude product was purified using strong cation exchanger (Dowex 50, H^+-form). Impurities were eluted with H_2O, product with 10% aq. pyridine. Pyridine was then removed using strong anion exchanger (Dowex 1, OH^--form). Impurities were eluted with H_2O and EtOH 1:1 mixture, product with H_2O and HCl mixture 1:1. The product-containing fractions were combined and evaporated. The resulting solid was dissolved in H_2O (10 ml) and EtOH (100 ml) was added to induce crystallization. Crystallization was finished on standing in the refrigerator overnight. Product was filtered off and dried under vacuum to yield white powder (0.66 g, 41%). NMR (D_2O, pD 2.9): ^1H δ = 2.26 (PCH_2CHP, 2H, m); 2.46 (PCH_2CHP, 1H, m); 3.42 [$N_{(ac)}$–CH_2CH_2–$N_{(ac)}$, 4H, s]; 3.50 [$N_{(ac)}$–CH_2CH_2–$N_{(bp)}$, 4H, s]; 3.56 [$N_{(ac)}$–CH_2CH_2–$N_{(bp)}$, 4H, s] 3.79 (NCH_2P, 2H, bs) 3.88 (N–CH_2–CO_2, 4H, s); $^{13}C\{^1H\}$ δ = 28.2 (PCH_2CHP$_2$, d, $^1J_{PC}$ 93.5 Hz); 34.2 (PCH_2CHP$_2$, t, $^1J_{PC}$ 117.7 Hz); 50.6 [$N_{(ac)}$–CH_2CH_2–$N_{(bp)}$, s]; 51.7 [$N_{(ac)}$–CH_2CH_2–$N_{(ac)}$, s]; 52.5 [$N_{(ac)}$–CH_2CH_2–$N_{(bp)}$, s]; 56.7 (NCH_2P, d, $^1J_{PC}$ 90.6 Hz); 58.0 (N–CH_2–CO_2, s); 173.3 (CO_2, s); $^{31}P\{^1H\}$ δ = 18.9 (PCH_2CHP, 2P, d, $^3J_{PP}$ 24.6 Hz); 33.1 ($P$$CH_2$CHP, 1P, t, $^3J_{PP}$ 24.6 Hz). MS (−): 509.8 $[M-H]^-$. Elemental analysis: found (calcd for $C_{13}H_{28}N_3P_3O_{13}\cdot 0.6$ HCl) C 29.4 (29.3); H 5.4 (5.4); N 7.3 (7.9).

4.9. Stock Solutions of Fe^{III} Complexes

Ligand (100 μmol) was dissolved in aq. $FeCl_3$ solution (90 μmol, 0.9 ml of 0.1 M solution), pH was slowly adjusted to 7 with 0.5 M aq. NaOH (precipitates may appear in this stage) and the solution was stirred at 80 °C for 1 h. Finally, water was added to reach final volume of 10.0 ml.

4.10. Adsorption Experiments

Hydroxyapatite (50 mg; Fluka, catalog no. 55496, 63 $m^2 g^{-1}$) was suspended in 1 M Tris–HCl buffer (0.30 ml; pH 7.5). Then, stock solution of Fe^{III} complex (10 mM, 0.06 to 0.60 ml) was added and the samples were diluted with water to obtain a final volume of 3.0 ml. The samples were stirred at 25 °C for 3 days. After filtration, concentration of the complex in the supernatant was quantified by UV–vis spectroscopy. Experimental data obtained at 250, 275 and 300 nm were treated by least-square fitting (Micromath Scientist software package) according to Langmuir adsorption isotherm.

4.11. $^{31}P\{^1H\}$ And ^{71}Ga NMR Complexation Studies

Solid $NOTAM^{BP}$ (25 mg, 51 μmol) was dissolved in 338 μl of 1 M aq. sodium chloroacetate buffer (experiments at pH 2 and pH 3) or 1 M aq. sodium acetate buffer (experiments at pH 4 and 5) and an equivalent amount of Ga^{III} ion (62 μl of 0.812 M solution) was added. For $NO2AP^{BP}$, the amounts were 25 mg of the solid ligand, 343 μl of buffer and 57 μl of 0.812 M Ga^{III} solutions. Samples were shaken and quickly transferred into a standard 5 mm NMR tube, and measured immediately (overall dead time was ~5 min) or left in an oil bath at the appropriate temperature for the given amount of time. Then, they were quickly cooled down to room temperature, the NMR spectrum was measured at 25 °C and heating was resumed again if necessary. Quantification was performed against ^{31}P or ^{71}Ga NMR standard in the insert tube. The times given in the text are those which the samples had spent at the given temperature.

4.12. Radiolabeling Studies

Gallium-68 (150–350 MBq) was obtained from a $^{68}Ge/^{68}Ga$ generator system (Eckert&Ziegler AG, Berlin). For *in vivo* experiments, ^{68}Ga labeling was performed in aq. HEPES buffer solution (pH 4, 0.125 M, 400 μl) by adding ^{68}Ga solution (400 μl) obtained by post-processing of the generator eluate via cation exchange method (52); the final pH of the solution was 3.75. Then, ligand (17 nmol, as stock solution with a concentration of 1 mg ml^{-1}) was added and the solution was shaken in a heating block for 10 min at 95 °C. After cooling, pH was adjusted to 7 by adding small amounts of 1 M aq. NaOH solution. Radiochemical yields of ^{68}Ga-complexes of the title ligands were 95–99%. For labeling studies under various pH conditions, labeling was carried out in deionized water (pure for pH = 2) or by adding smaller amounts of buffer solution (i.e. decreasing buffer capacity of the final solution) to obtain the appropriate final pH. Radiochemical yields were determined by silica TLC (Merck) using a solvent mixture consisting of 2 parts of A (conc. aq. HCl–acetone–water, 100 μl:1 ml:1 ml) and 1 part of B (pure acetylacetone). The activity was measured on a Canberra Packard Instant Imager. Free ^{68}Ga migrates as an acetylacetonate complex with solvent front. *In-cage* complexes stay on the baseline (^{68}Ga-phosphonates: $R_f = 0.0–0.1$; ^{68}Ga-acac: $R_f = 0.8–0.9$; for details, see Supporting Information). Radiochemical yields were also determined by radio-HPLC (Merck-Hitachi-LaChrom, Gabi-Raytest) using a LiChrosphere C_{18} (CS-Chromatographie, Germany) column. The reaction solution (10 μl) was added to 50 μl of deferoxamine (DFO) solution (0.1 mg ml^{-1}) in 0.1 M NaAc buffer (pH 4.0). ^{68}Ga-labeled bis(phosphonates) showed a weak retention, while [^{68}Ga]DFO showed a retention time of 10 min (Figs S11–S13 in the Supporting Information). [^{68}Ga]NOTA and [^{68}Ga]DOTA complexes were synthesized using the method described above with 10 μg of each chelator. [^{68}Ga]$DO3AP^{BP}$ was labeled with ^{68}Ga with a different method. $DO3AP^{BP}$ was dissolved in deioinized water with a concentration of 1 mg ml^{-1}. This solution (17 μl, that is, 17 μg $DO3AP^{BP}$) was added to a 0.25 M ammonium acetate buffer (500 μl, pH 5). Post-processed ^{68}Ga solution (400 μl) was added and the mixture was shaken in a heating block for 20 min. Labeling at lower pHs was carried out by using less concentrated buffer solutions. Labeling at pH 1–2 was done using deionized water as the reaction solvent.

4.13. Evaluation of Hydrolysis During Radiolabeling

Radiolabeling was done as described above (95 °C, pH 4.5, 15 min) and the solution was analyzed by HPLC with Merck–Hitachi Lachrom equipment, Raytest Gabi radiodetector and Nucleosil 100-5 NH_2 phase in a 125× 4.6 mm column. Elution: 0–30 min, 100% 0.1 M aq. NaH_2PO_4 (pH 4.5); 31–60 min, 100% 0.1 M aq. Na-citrate (pH 4.5); and 60–65 min, 100% 0.1 M aq. NaH_2PO_4 (pH 4.5).

4.14. Binding Studies of ^{68}Ga–ligand Complexes on Hydroxyapatite

HAP (20 mg, Sigma-Aldrich, reagent grade powder) was incubated in isotonic saline (1 ml) for 24 h. The test was performed by addition of 50 μl of ^{68}Ga-bis(phosphonates) solution (prepared as given above) to the HAP suspension. After vortexing for 10 s, the suspension was incubated for 10 min at room temperature. The samples were centrifuged and the supernatant was removed. The HAP fraction was washed with isotonic saline (0.5 ml). ^{68}Ga radioactivity in the combined liquids and that of the HAP fraction were measured in a curiemeter (Aktivimeter Isomed 2010, MED Nuklear-Medizintechnik Dresden GmbH). ^{68}Ga-complex binding to HAP was determined as percent of ^{68}Ga absorbed to HAP (53).

4.15. Animals, Feeding, Husbandry, and Animal Preparation

Experiments were conducted according to institutional guidelines and German animal welfare regulations. The experimental procedure used conforms to European Convention for the Protection of Vertebrate Animals used for Experimental and other Scientific Purposes (ETS no. 123) and to the Deutsches Tierschutzgesetz. Male Wistar rats (Charles River Laboratories International Inc.) weighing 130 ± 15 g (mean ± SD, $n = 10$) for *ex vivo* organ distribution, 536 and 346 g for microPET-imaging ($n = 2$), were anesthetized with isoflurane. Animals were put in a supine position and placed under an infrared lamp to maintain body temperature.

4.16. Biodistribution Studies

Biodistribution studies were performed in male Wistar rats (120–140 g). Each study group contained five rats. The rats were injected intravenously, each with ^{68}Ga-labeled compound in

saline (0.5 ml); for [^{68}Ga]NO3AP^{BP}, 13.5 ± 5.8 MBq, body weight 142 ± 3 g; for [^{68}Ga]NOTAM^{BP}, 10.5 ± 1.9 MBq, body weight 128 ± 7 g. Animals were sacrificed at 60 min after injection. Organs and tissues of interest were excised rapidly and weighed, and radioactivity was determined using a Wallac WIZARD2 automatic gamma counter (Perkin Elmer, Germany). Activity of the tissue samples was decay- and background-corrected.

4.17. Small Animal MicroPET

In vivo small animal microPET imaging of male Wistar rats (350–540 g) was carried out under general anesthesia of the rats that was induced with inhalation of 10% and maintained with inhalation of 6.5% isoflurane in 30% oxygen/air. Rats were positioned supine in the scanner (Siemens microPET Focus 120). In the microPET experiments, [^{68}Ga]NO2AP^{BP} (32 MBq for the first animal, 536 g and 31 MBq for the second animal, 346 g in isotonic saline, 0.5 ml) was administered intravenously using a needle catheter into the tail vein. No correction for partial volume effects was applied. Image volume data were converted to Siemens ECAT7 format for further processing. Image files were then processed using a Pmod software (PMOD Technologies Ltd).

4.18. Statistical Analysis

All data were expressed as mean ± SD. Groups were compared using t-test. All statistical tests were two-tailed, with a *p*-value of <0.05 representing significance, except for comparison of [^{68}Ga]NO2AP^{BP}and [^{68}Ga]EDTMP in HAP-binding experiment, which showed a P-value of 0.052. No differences were observed for [^{68}Ga]NO2AP^{BP} and [^{68}Ga]DO3AP^{BP} in HAP-binding experiment ($p = 0.7$); for the values, see the Supporting Information (Table S1).

Acknowledgment

Support from the Grant Agency of the Czech Republic (13-08336S) and the Grant Agency of the Charles University in Prague (no. 19310) is acknowledged. The work was carried out in the framework of COST TD1004 and TD1007 Actions. We are grateful to Nicole Bausbacher and Barbara Biesalski (Mainz Universiy) for performing the animal experiments.

REFERENCES

1. Rösch F, Riss PJ. The renaissance of the ^{68}Ge/^{68}Ga radionuclide generator initiates new developments in ^{68}Ga radiopharmaceutical chemistry. Curr Top Med Chem 2010; 10: 1633–1668.
2. Fani M, André JP, Mäcke HR. ^{68}Ga-PET: a powerful generator-based alternative to cyclotron-based PET radiopharmaceuticals. Contrast Media Mol Imag 2008; 3: 53–63.
3. Wadas TJ, Wong EH, Weisman GR, Anderson CJ. Coordinating radiometals of copper, gallium, indium, yttrium, and zirconium for PET and SPECT imaging of disease. Chem Rev 2010; 110: 2858–2902.
4. Velikyan I. Positron Emitting [^{68}Ga]Ga-based imaging agents: chemistry and diversity. Med Chem 2011; 7: 345–372.
5. Breeman WAP, de Blois E, Chan HS, Konijnenberg M, Kwekkeboom DJ, Krenning EP. ^{68}Ga-labeled DOTA-peptides and ^{68}Ga-labeled radiopharmaceuticals for Positron Emission Tomography: current status of research, clinical applications, and future perspectives. Semin Nucl Med 2011; 41: 314–321.
6. Bartholomae MD. Recent developments in the design of bifunctional chelators for metal-based radiopharmaceuticals used in positron emission tomography. Inorg Chim Acta 2012; 389: 36–51.
7. Banerjee SR, Pomper MG. Clinical applications of gallium-68. Appl Radiat Isotop 2013; 76: 2–13.
8. Zhang S, Gangal G, Uludag H. Magic bullets' for bone diseases: progress in rational design of bone-seeking medicinal agents. Chem Soc Rev 2007; 36: 507–531.
9. Kubíček V, Lukeš I. Bone-seeking probes for optical and magnetic resonance imaging. Fut Med Chem 2010; 2: 521–531.
10. Palma E, Correia JDG, Campello MPC, Santos I. Bisphosphonates as radionuclide carriers for imaging or systemic therapy. Mol BioSyst 2011; 7: 2950–2966.
11. Fleisch H. Bisphosphonates in Bone Disease, 4th edn. Academic Press: London, 2000.
12. Kubíček V, Rudovský J, Kotek J, Hermann P, vander Elst L, Muller RN, Kolar ZI, Wolterbeek H T, Peters JA, Lukeš I. A bisphosphonate monoamide analogue of DOTA: a potential agent for bone targeting. J Am Chem Soc 2005; 127: 16477–16485.
13. Vitha T, Kubíček V, Hermann P, vander Elst L, Muller RN, Kolar ZI, Wolterbeek HT, Breeman WAP, Lukeš I, Peters JA. Lanthanide(III) complexes of bis(phosphonate) monoamide analogues of DOTA: bone-seeking agents for imaging and therapy. J Med Chem 2008; 51: 677–683.
14. Vitha T, Kubíček V, Kotek J, Hermann P, vander Elst L, Muller RN, Lukeš I, Peters JA. Gd(III) complex of a monophosphinate-bis (phosphonate) DOTA analogue with a high relaxivity. Lanthanide (III) complexes for imaging and radiotherapy of calcified tissues. Dalton Trans 2009; 3204–3214.
15. Liu W, Hajibeigi A, Lin M, Rostollan CL, Kovács Z, Öz OK, Sun X. An osteoclast-targeting agent for imaging and therapy of bone metastasis. Bioorg Med Chem Lett 2008; 18: 4789–4793.
16. Ogawa K, Kawashima H, Shiba K, Washiyama K, Yoshimoto M, Kiyono Y, Ueda M, Mori H, Saji H. Development of [^{90}Y]DOTA-conjugated bisphosphonate for treatment of painful bone metastases. Nucl Med Biol 2009; 36: 129–135.
17. Suzuji K, Satake M, Suwada J, Oshikiri S, Ashino H, Dozono H, Hino A, Kasahara H, Minamizawa T. Synthesis and evaluation of a novel ^{68}Ga-chelate-conjugated bisphosphonate as a bone-seeking agent for PET imaging. Nucl Med Biol 2011; 38: 1011–1018.
18. Fellner M, Baum RP, Kubíček V, Hermann P, Lukeš I, Prasat V, Rösch F. PET/CT imaging of osteoblastic bone metastases with ^{68}Ga-bisphosphonates: first human study. Eur J Nucl Med Mol Imag 2010; 37: 834.
19. Fellner M, Biesalski B, Bausbacher N, Kubíček V, Hermann P, Rösch F, Thews O. ^{68}Ga-BPAMD: PET-imaging of bone metastases with a generator based positron emitter. Nucl Med Biol 2012; 39: 993–996.
20. Baum RP, Kulkarni, HR. Theranostics: from molecular imaging using ^{68}Ga labeled tracers and PET/CT to personalized radionuclide therapy – the Bad Berka experience. Theranostics 2012; 2: 437–447.
21. Vitha T, Kubíček V, Hermann P, Kolar ZI, Wolterbeek HT, Peters JA, Lukeš I. Complexes of DOTA-bisphosphonate conjugates: probes for determination of adsorption capacity and affinity constants of hydroxyapatite. Langmuir 2008; 24: 1952–1958.
22. Rill C, Kolar ZI, Kickelbick G, Wolterbeek HT, Peters JA. Kinetics and thermodynamics of adsorption on hydroxyapatite of the [^{160}Tb] terbium complexes of the bone-targeting ligands DOTP and BPPED. Langmuir 2009; 25: 2294–2301.
23. Heppeler A, Froidevaux S, Mäcke HR, Jermann E, Béhé M, Powell P, Hennig M. Radiometal-labelled macrocyclic chelator-derivatised somatostatin analogue with superb tumour-targeting properties and potential for receptor-mediated internal radiotherapy. Chem Eur J 1999; 5: 1974–1981.
24. Niu W, Wong EH, Weisman GR, Peng Y, Anderson CJ, Zakharov LN, Golen JA, Rheingold AL. Structural and dynamic studies of zinc, gallium, and cadmium complexes of a dicarboxylate pendant-armed cross-bridged cyclen. Eur J Inorg Chem 2004; 3310–3315.
25. Cola NA, Rarig, Jr. RS, Ouellette W, Doyle RP. Synthesis, structure and thermal analysis of the gallium complex of 1,4,7,10-tetraazacyclododecane-*N,N′,N″,N‴*-tetraacetic acid (DOTA). Polyhedron 2006; 25: 3457–3462.
26. Yang C-T, Li Y, Liu S. Synthesis and structural characterization of complexes of a DO3A-conjugated triphenylphosphonium cation with diagnostically important metal ions. Inorg Chem 2007; 46: 8988–8997.
27. Kubíček V, Havlíčková J, Kotek J, Tircsó G, Hermann P, Tóth É, Lukeš I. Gallium(III) complexes of DOTA and DOTA-monoamide: kinetic and thermodynamic studies. Inorg Chem 2010; 49: 10960–10969.
28. Šimeček J, Schulz M, Notni J, Plutnar J, Kubíček V, Havlíčková J, Hermann P. Complexation of metal ions with TRAP (1,4,7-triazacyclononane phosphinic acid) ligands and 1,4,7-triazacyclononane-1,4,7-triacetic

acid: phosphinate-containing ligands as unique chelators for trivalent gallium. Inorg Chem 2012; 51: 577–590.
29. Notni J, Hermann P, Havlíčková J, Kotek J, Kubíček V, Plutnar J, Loktionova N, Riss PJ, Rösch F, Lukeš I. A triazacyclononane-based bifunctional phosphinate ligand for the preparation of multimeric ^{68}Ga tracers for positron emission tomography. Chem Eur J 2010; 16: 7174–7185.
30. Shetty D, Jeong JM, Ju CH, Kim YJ, Lee J-Y, Lee Y-S, Lee DS, Chung J-K, Lee MC. Synthesis and evaluation of macrocyclic amino acid derivatives for tumor imaging by gallium-68 positron emission tomography. Bioorg Med Chem 2010; 18: 7338–7347.
31. Shetty D, Choi SY, Jeong JM, Hoigebazar L, Lee Y-S, Lee DS, Chung J-K, Lee MC, Chung YK. Formation and characterization of gallium(III) complexes with monoamide derivatives of 1,4,7-triazacyclononane-1,4,7-triacetic acid: a study of the dependency of structure on reaction pH. Eur J Inorg Chem 2010; 5432–5438.
32. Hoigebazar L, Jeong JM, Choi SY, Choi JY, Shetty D, Lee Y-S, Lee DS, Chung J-K, Lee MC, Chung YK. Synthesis and characterization of nitroimidazole derivatives for ^{68}Ga-labeling and testing in tumor xenografted mice. J Med Chem 2010; 53: 6378–6385.
33. de Sá A, Matias ÁA, Prata MIM, Geraldes CFGC, Ferreira PMT, André JP. Gallium labeled NOTA-based conjugates for peptide receptor-mediated medical imaging. Bioorg Med Chem Lett 2010; 20: 7345–7348.
34. Meckel M, Fellner M, Thieme N, Bergmann R, Kubíček V, Rösch F. *In vivo* comparison of DOTA based ^{68}Ga-labelled bisphosphonates for bone imaging in non-tumour models. Nucl Med Biol 2013; 40: 823–830.
35. Blake AJ, Fallis IA, Gould RO, Persons S, Ross SA, Schröder M. Selective derivatisation of azamacrocycles. J Chem Soc Dalton Trans 1996; 4379–4387.
36. Huskens J, Sherry AD. Synthesis and characterization of 1,4,7-triazacyclononane derivatives with methylphosphinate and acetate side chains for monitoring free Mg^{II} by ^{31}P and ^{1}H NMR spectroscopy. J Am Chem Soc 1996; 118: 4396–4404.
37. Chong H-S, Song HA, Birch N, Le T, Lim S, Ma X. Efficient synthesis and evaluation of bimodal ligand NETA. Bioorg Med Chem Lett 2008; 18: 3436–3439.
38. Riss PJ, Kroll C, Nagel V, Rösch F. NODAPA-OH and NODAPA-$(NCS)_n$: synthesis, ^{68}Ga-radiolabelling and in vitro characterization of novel versatile bifunctional chelators for molecular imaging. Bioorg Med Chem Lett 2008; 18: 5364–5367.
39. Shetty D, Choi SY, Jeong JM, Lee JY, Hoigebazar L, Lee Y-S, Lee DS, Chung J-K, Lee MC, Chung YK. Stable aluminium fluoride chelates with triazacyclononane derivatives proved by X-ray crystallography and ^{18}F-labeling study. Chem Commun 2011; 47: 9732–9734.
40. Matczak-Jon E, Videnova-Adrabinska V. Supramolecular chemistry and complexation abilities of diphosphonic acids. Coord Chem Rev 2005; 249: 2458–2488.
41. Kubíček V, Kotek J, Hermann P, Lukeš I. Aminoalkyl-bis(phosphonates): their complexation properties in solution and in the solid state. Eur J Inorg Chem 2007; 333–344.
42. Broan C, Cox JP, Craig AS, Kataky R, Parker D, Harrison A, Randall AM, Ferguson G. Structure and solution stability of indium and gallium complexes of 1,4,7-triazacyclononanetriacetate and of yttrium complexes of 1,4,7,10-tetraazacyclododecanetetraacetate and related ligands: kinetically stable complexes for use in imaging and radioimmunotherapy. X-Ray molecular structure of the indium and gallium complexes of 1,4,7-triazacyclononane-1,4,7-triacetic acid. J Chem Soc, Perkin Trans 2 1991; 87–99.
43. André JP, Mäcke HR, Zehnder M, Macko L, Akyel KG. 1,4,7-triazacyclononane-1-succinic acid-4,7-diacetic acid (NODASA): a new bifunctional chelator for radio gallium-labelling of biomolecules. Chem Commun 1998; 1301–1302.
44. Lukeš I, Kotek J, Vojtíšek P, Hermann P. Complexes of tetraazacycles bearing methylphosphinic/phosphonic acid pendant arms with copper(II), zinc(II) and lanthanides(III). A comparison with their acetic acid analogues. Coord Chem Rev 2001; 216&217: 287–312.
45. Notni J, Šimeček J, Hermann P, Wester H-J. TRAP, a powerful and versatile framework for gallium-68 radiopharmaceuticals. Chem Eur J 2011; 17: 14718–14722.
46. Šimeček J, Notni J, Zemek O, Hermann P, Wester H-J. A monoreactive bifunctional triazacyclononane phosphinate chelator with high selectivity for gallium-68. ChemMedChem 2012; 7: 1375–1378.
47. Šimeček J, Hermann P, Wester, H-J, Notni J. How is ^{68}Ga labeling of macrocyclic chelators influenced by metal ion contaminants in ^{68}Ge/^{68}Ga generator eluates? ChemMedChem 2013; 8: 95–103.
48. Notni J, Plutnar J, Wester H-J. Bone-seeking TRAP conjugates: surprising observations and their implications on the development of gallium-68-labeled bisphosphonates. EJNMMI Res 2012; 2: 13.
49. Wieghardt K, Bossek U, Chaudhuri P, Herrmann W, Menk BC, Weiss J. 1,4,7-Triazacyclononane-*N*,*N*′,*N*″-triacetate (TCTA), a new hexadentate ligand for divalent and trivalent metal ions. Crystal structures of $[Cr^{III}(TCTA)]$, $[Fe^{III}(TCTA)]$, and $Na[Cu^{II}(TCTA)]\cdot 2NaBr\cdot 8H_2O$. Inorg Chem 1982; 21: 4308–4314.
50. Dixon DA, Shang M, Lappin AG. Effects of electronic structure on chiral induction in outer-sphere electron transfer reactions of complexes with the C_3 symmetric ligand, 1,4,7-triazacyclononane-1,4,7-tris[2′(*R*)-2′-propionate]$^{3-}$. Inorg Chim Acta 1999; 290: 197–206.
51. Chang CA, Francesconi LC, Malley MF, Kumar K, Gougoutas JZ, Tweedle MF. Synthesis, characterization, and crystal structures of M(DO3A) (M = Fe, Gd) and Na[M(DOTA)] (M = Fe, Y, Gd). Inorg Chem 1993; 32: 3501–3508.
52. Zhernosekov KP, Filosofov DV, Baum RP, Aschoff P, Bihl H, Razbash AA, Jahn M, Jennewein M, Rösch F. Processing of generator-produced ^{68}Ga for medical application. J Nucl Med 2007; 48: 1741–1748.
53. Fellner M, Riss P, Loktionova N, Zhernosekov KP, Thews O, Geraldes CFGC, Kovács Z, Lukeš I, Rösch F. Comparison of different phosphorus-containing ligands complexing ^{68}Ga for PET-imaging of bone metabolism. Radiochim Acta 2011; 99: 43–51.

Supporting information

Additional supporting information may be found in the online version of this article at the publisher's web site.

